Elastic and quasielastic neutron scattering studies in KBr:KCN mixed crystals

A. Loidl[1], T. Schräder[1], K. Knorr[1], R. Böhmer[1], B. Mertz[1], G.J. McIntyre[2]*, T. Vogt[2], H. Mutka[2], M. Müllner[3], H. Jex[4], and S. Haussühl[5]

[1] Institut für Physik, Universität Mainz, Federal Republic of Germany
[2] Institut Laue Langevin, Grenoble, France
[3] Institut für Kernphysik, Universität Frankfurt, Federal Republic of Germany
[4] Abteilung Physik, Universität Ulm, Federal Republic of Germany
[5] Institut für Kristallographie, Universität zu Köln, Federal Republic of Germany

Neutron scattering studies in $(KBr)_{1-x}(KCN)_x$ mixed crystals are presented utilizing powder diffraction, single crystal diffraction and time-of-flight techniques. For $x>0.6$ $(KBr)_{1-x}(KCN)_x$ crystals exhibit ferroelastic and ferroelectric low-temperature phases. Crystals with $x<0.6$ undergo transitions into an orientational glass state. Here we present a detailed phase diagram including new results for $x=0.85$ and $x=0.65$. For the latter system a stable rhombohedral low-temperature phase has been detected where the orientational disorder of the plastic phase is only partly removed and quadrupolar relaxations between three body diagonals are still possible. From the powder diffraction experiments we determined further the concentration dependence of the static Debye-Waller factors which can be explained by an interplay of the rotation-translation and the rotation-random strain coupling. With single crystal diffraction techniques we studied the diffuse scattered intensities which are directly related to the order parameter of the glass state. The temperature dependence of the quasielastic intensities near the critical concentration shows a strong increase for $T<110$ K indicative for a freezing-in of shear fluctuations which is a characteristic feature of a non-ergodic instability. This phenomenon appears for ordering ($x=0.65$) and for non-ordering, glassy compounds. A further anomaly in $(KBr)_{0.43}(KCN)_{0.57}$ at 75 K is interpreted in terms of a residual elastic ordering process. With high-resolution time-of-flight techniques we analysed the dynamic structure factor for $x=0.57$. We demonstrate that the central peak consists of a static and a dynamic component. The results are compared with mode coupling theories which describe the glass transition in supercooled liquids.

I. Introduction

During the last decade glassy crystals which are a new class of disordered materials have attracted considerable attention. The common signatures of these systems are relaxation phenomena of the orientational degrees of freedom which are analogous to those observed in canonical glasses and in spin glasses and low temperature thermodynamic, elastic and dielectric properties which are characteristic of amorphous systems. Orientational glasses are mixed crystals which exhibit paraelectric or paraelastic high temperature phases. But while the pure compounds undergo structural phase transitions into elastically and electrically ordered low temperature phases, the phase transitions in the mixed crystals are suppressed over a wide concentration range. There long range orientational order is prevented either through competing interactions and frustration effects or through random strains.

The following classes of mixed crystals exhibit a glassy state at low temperatures:
i) mixed molecular crystals where the anisotropic molecules are substituted by isotropic atoms or ions:

* Present address: The Studsvik Neutron Research Laboratory, University of Uppsala, S-61182 Nyköping, Sweden

Ortho-para hydrogen mixtures [1], KCN:KBr [2–4], N_2:Ar [5–7] and CH_4:Kr [8] are the most prominent examples. Off-center systems like $KTaO_3$:Li(Na) [9] where the thermal hopping of the off-center ions can be described in terms of a pseudospin formalism are also related to this group. In these glassy systems the freezing-in of the orientational degrees of freedom is still a cooperative phenomenon, but long range orientational order is suppressed through an interplay of random fields and frustrated interactions. In addition, in some compounds the translational order in the glass state is highly disturbed by strong rotation-translation coupling forces. In these cases the low temperature state can be viewed as intermediate between the crystalline and the amorphous state.

ii) mixed dipolar crystals where the two components exhibit ferroelectric and antiferroelectric interactions: In Rb:$NH_4H_2PO_4$ [10] a frustrated ground state is believed to occur via the two competing electric interactions and

iii) molecular crystals with strong random fields like NaCN:KCN [11, 12]. At intermediate concentrations these mixed crystals can be described purely within a random field model and collective freezing phenomena can be neglected.

All these systems exhibit very similar x, T-phase diagrams with a large concentration range which is characterized by frozen-in orientational correlations but which shows no long range elastic or electric order at low temperatures. According to the dominant interactions glassy crystals are termed dipolar (frozen-in electric disorder) or quadrupolar (frozen-in elastic disorder) glasses. The name orientational glass characterizes the frozen in orientational disorder, but pays no attention to the breakdown of the long range translational order of the center of mass lattice which depends on the strength of the rotation-translation coupling and plays an outstanding role in the cyanide glasses.

The alkali cyanide-alkali halide mixed crystals $(MX)_{1-x}(MCN)_x$, where M is the alkali metal and X an halogen ion, are model systems for structural phase transitions [13–16] and for transitions into an orientational glass state [2, 17–20]. Above a critical concentration x_c these systems display ferroelastic phase transitions from a high temperature rotator phase to orientationally ordered low temperature phases [21–28]. At low temperatures a rich variety of crystallographic phases exhibiting orientational (quadrupolar) and electric (dipolar) long range order have been reported [21–28]. The elastic phase transitions are triggered by a bilinear coupling of the molecular reorientations to the lattice strains yielding an effective quadrupolar interaction between neighbouring CN^- molecules. The electric ordering is driven by direct dipolar interaction forces. However, below x_c the structural phase transitions are replaced by frequency dependent glass transitions [19, 20]. The freezing process is a cooperative effect driven by strain mediated CN^- – CN^- interactions, but long range orientational order cannot be established. At present it is unclear as to what extent long range orientational order is suppressed by random fields introduced by the substitutional impurity atoms X as opposed to through frustration effects like in spin classes [29, 30]. In the cyanide glasses frustration is believed to occur via the interplay of dilution, yielding a site disorder of the molecules and the anisotropic quadrupolar interactions.

The quadrupolar freezing process is indicated by cusps in the quadrupolar susceptibility or equivalently by minima in the temperature dependence of the elastic properties [2, 17–19, 31–33]. The low temperature state, termed quadrupolar or orientational glass, is characterized by frozen-in orientational correlations and frozen-in lattice strains [2, 17, 34–36]. The central line in inelastic neutron scattering experiments [2, 17, 29, 33], the line width broadening of the Bragg reflections in X-ray measurements [23, 24] and the increase of the distribution width of the electric field gradient in NMR experiments [24, 29] are related to the order parameter, which is the characteristic signature of the glass state [37, 38]. The appearance of these phenomena can qualitatively be explained by a breaking of the long range translational order. Or, to be more specific, the diffraction pattern can be interpreted as being due to a distribution of lattice parameters around the high-temperature cubic lattice [34]. Thus the glass state can be described as a network of clusters, which exhibit a distribution of shear deformations centered around zero strain.

A large number of experimental and theoretical investigations focused on the low temperature properties of glassy crystals. The cyanide glasses, especially, exhibit low temperature thermal [39], ultrasonic [40] and dielectric properties [41] which are analogous to those found in canonical glasses and in amorphous solids [42, 43]. In amorphous systems the low temperature properties appear to be dominated by two level tunnelling systems. The tunnelling center theories [42, 43] had enormous success in explaining the temperature and time dependence of the specific heat. In the glassy state of KBr:CN an attempt was made to identify the tunnelling centers with dipolar reorientations (180° flips) of the CN^- ions within the locally distorted crystalline potential [44]. However, in a recent experimental study of N2:Ar:CO mixtures it was demonstrated that dipolar relaxations of the CO molecules do not contribute to the low temperature specific heat [45].

Theoretically K.H. Michel described the relaxation phenomena in the cyanide glasses within the framework of a random field model [37]. Later on he extended this theory including a collective freezing which results in a nonergodic instability [38]: near a ferroelastic phase transition with a soft mode behaviour even small random fields pin the dynamic modes which are characterized by very weak restoring forces. These weak random strains freeze-in critical fluctuations in a lattice that is close to a structural instability. Hence, the glass transition is characterized by the freezing of long wavelength orientational excitations coupled to the lattice strains. Recent molecular dynamics calculations demonstrated that the competition of random strain-rotation coupling and rotation-translation coupling indeed can explain the variety of low temperature states as observed in KBr:CN [46, 47].

Mean field calculations on quadrupolar glasses with infinite random Gaussian interactions [48, 49] and Monte Carlo simulations with nearest neighbour interactions [50] have been performed. These studies focused on the random bond disorder and disregarded the random field problem completely.

Following the arguments outlined above two effects are important in forming a glassy state: *i*) frustration effects due to the anisotropic interactions between site disordered quadrupoles and *ii*) random field effects caused by the substitutional impurity atoms. Experimentally these two limiting cases can be discriminated by measuring the order parameter of the glass state. In random field systems the order parameter is a smooth function of temperature. In frustrated systems a non-zero order parameter only exists below a well defined glass transition temperature. The latter case is the analog to the Edwards-Anderson order parameter in spin glasses. Therefore, experimentally the temperature dependence of the central peak allows for a conclusive discrimination between these two models. In the single crystal diffraction study we will focus especially on this point.

In this paper we summarize detailed neutron scattering investigations of $(KBr)_{1-x}(KCN)_x$. Using powder diffraction techniques we studied the structure of the low temperature phases over the complete concentration range. Results are presented which document a single rhombohedral phase for $x=0.65$ and which show that within this phase the degrees of freedom for the molecular orientations are reduced from four to three only, giving a large residual entropy at zero temperature. We show detailed results for the temperature and the concentration dependence of the Debye-Waller factors. With single crystal diffraction experiments we investigated the distribution and the temperature dependence of the frozen-in strain fields which are a direct measure of the order parameter of the glass state. We show that the diffuse scattered intensities which appear near the Bragg reflections exhibit a sharp increase at low temperatures indicating a nonergodic instability. In addition, well defined discontinuities in the T-dependence of the line widths and of the integrated intensities were detected. We speculate about the physical origin of these anomalies and their connection to the establishment of residual order within the glass state. Finally, we show preliminary results of inelastic time-of-flight experiments in mixed crystals with concentrations $x=0.2$ and $x=0.57$. Here we can present the first indications that the central peak consists of two contributions: a truly static component and in addition a dynamic component with a finite width. This observation supports recent theoretical approaches from K.H. Michel [38] showing that the order parameter of the glass state consists of a static component due to the coupling of the orientational reorientations to the random strain fields and of a dynamic part which describes the freezing-in of critical fluctuations.

II. Experimental results and analysis

Most of the $(KBr)_{1-x}(KCN)_x$ single crystals that have been investigated in the present neutron scattering studies have been grown by one of the authors (S. Haussühl). In addition, mixed crystals with concentrations $x=0.41$ and 0.2 were purchased from the Crystal Growth Laboratory of the University of Utah. Detailed studies were performed on crystals with concentrations $x=1$, 0.85, 0.65, 0.57, 0.53, 0.41 and 0.2. The x-values cited in this article always denote the actual CN^- concentration in the solid phase which was determined gravimetrically. Due to the shape of the liquidus-solidus phase boundaries in the KBr:KCN system [51] the actual CN concentration in the crystalline state is significantly lower than that in the melt. Figure 1 shows the dependence of the molar CN concentration in the solid state from that in the melt. The results are shown for the crystals grown in Utah and in Köln. The agreement is very satisfactory. Figure 1 demonstrates that the difference in the CN concentration between the liquid and the solid state reaches as much as 10%. In Fig. 2 we show the concentration dependence of the cell volume of the mixed crystals as determined at 5 K and at 295 K (here the unit cell contains $4\,K^+$ and $4\,Br^-/CN^-$ ions). The results of the present experiments are compared to data cited in the literature [22, 52]. At high and at low temperatures the concentration dependence of the lattice parameters is smooth. However, at room temperature small but significant deviations

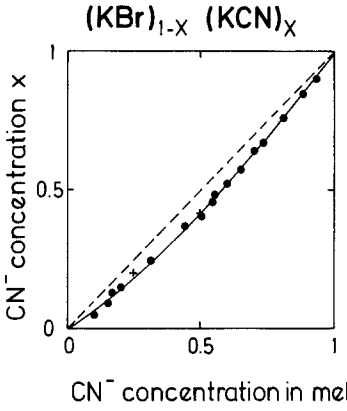

Fig. 1. Nominal molar CN^- concentration x of mixed $(KBr)_{1-x}(KCN)_x$ crystals versus the molar composition of the melt: crystals grown in Köln (●); crystals purchased from Utah (+)

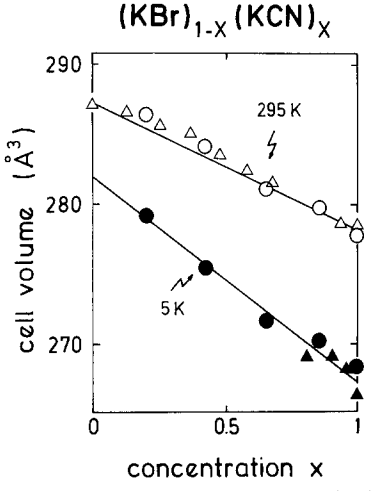

Fig. 2. Cell volume of KBr:KCN mixed crystals at room temperature (295 K, empty symbols) and at low temperatures (5 K–10 K, full symbols) versus concentration x: this work: (●, ○); Kaack (X-ray data; Ref. 46): (△); Rowe et al. (neutron data; Ref. 20): (▲)

from Vegard's law become apparent: the cell volumes of the mixed crystals are systematically shifted towards larger values compared to the predictions of a linear interpolation. Figure 2 also indicates that the overall thermal expansion for KCN is significantly larger than for KBr.

For the powder diffraction study and for the time-of-flight investigation the samples were prepared by grinding solid boules in an Argon atmosphere and then were loaded in Vanadium cans. For the single crystal diffraction study samples with a volume of approximately 50 mm^3 were cut from large single crystals. All the investigations were performed at the High Flux Reactor of the Institut Laue-Langevin in Grenoble.

So far a number of studies of the low temperature phases of the KBr:KCN system have been made by X-ray and neutron powder diffraction (Rowe, Rush and Chesser [21]; Rowe, Rush and Susmann [22]; Knorr and Loidl [23]; Rowe, Bouillot, Rush and Lüty [25]; Bouillot, Rowe and Rush [26] and Bourson, Gorczyca and Durand [27]). Transition temperatures have been determined by Suga, Matsuo and Seki [53]; Lüty [54]; Matsuo, Kishimoto, Suga and Lüty [55] and by Mertz and Loidl [28] by calorimetry. The phase diagrams proposed so far [23, 25, 27, 28] differ considerably. E.g. in the X-ray diffraction work of [27] no rhombohedral phases were detected. Furthermore, several of the powder diffraction studies have suggested mixed phases, although this might be due to concentration gradients that cross the nearly vertical phase lines. In addition the structures for several concentrations depend sensitively on the sample history [56] in a similar manner to pure KCN [57].

Nevertheless, all the phase diagrams of the alkali halide-alkali cyanide mixtures investigated so far exhibit a fascinating polymorphism. The structural polymorphism of these mixed molecular systems is a striking feature of the phase diagrams and is reminescent of the structural polymorphism in a number of canonical glasses. It is however still an open question whether or not the tendency to form different structural phases is directly related to the tendency to form a glassy state. The ability of many covalent liquids to form a glass appears to be a direct consequence of the indifference of the crystalline network structure with respect to distortions [58].

Above the critical concentration $x_c = 0.6$ all the low temperature phases exhibit orientational (elastic) order but only the crystals exhibiting an orthorhombic structure undergo an electric ordering process yielding a perfect head to tail order of the CN^- molecules at low temperatures. The other structures are dipolar disordered down to the lowest temperatures. Below x_c no anomalies in the specific heat versus temperature curve can be detected [28]. In this concentration range no long range orientational order is established and, on the average, the center of masses still form a cubic lattice with short range orientational order and local shear distortions.

A. Powder diffraction study

In view of the uncertainties in the phase diagram, we performed further neutron diffraction studies at a number of concentrations, partly to complete further the phase diagram and partly to confirm other workers findings on the possible mixed phases. The neutron diffraction patterns were recorded on the

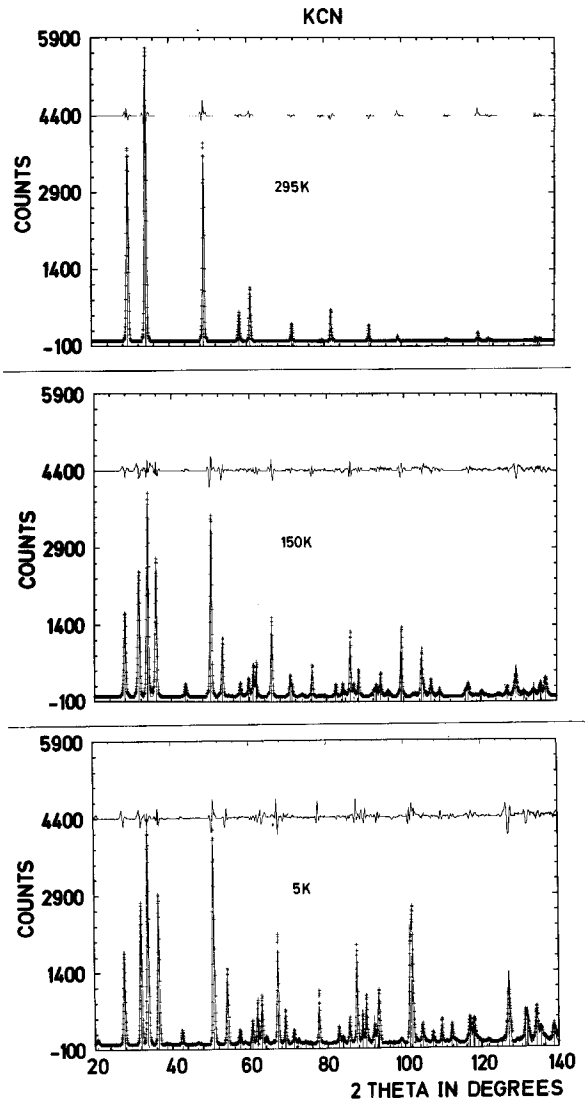

Fig. 3. Neutron powder spectra of KCN at different temperatures. The continuous lines are the best fits of a Rietveld structural refinement. The difference spectra between the best fits and the data points are also shown

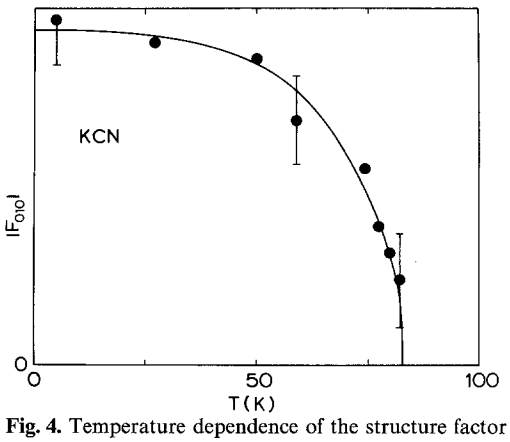

Fig. 4. Temperature dependence of the structure factor of the (010) superstructure reflection of the primitive orthorhombic phase of pure KCN as determined by neutron powder diffraction. The solid line corresponds to a spin-1/2 Brillouin function

multi-detector diffractometer D1A located on a thermal neutron guide. The incident wave length was 1.91 Å. For all samples the temperature was either decreased monotonically from 295 K, or set immediately to 5 K and then increased monotonically. All the data have been analyzed using the Rietveld technique of refinement [59, 60]. The Figs. 3 and 5–7 show the diffraction profiles for concentrations $x=1$, 0.85, 0.65 and 0.41 at different temperatures. The results can be summarized as follows:

$x=1$: for pure KCN we find the well known low temperature phases [21–23]. A ferroelastically ordered phase with orthorhombic symmetry (Immm) exists in a temperature range $168\,\mathrm{K} \leqq T \leqq 83\,\mathrm{K}$. At 83 K the head-to-tail disorder of the CN^- dipoles is removed by a second order phase transition into a primitive orthorhombic structure (Pmnm). The onset of antiferroelectric order can be seen by the appearance of superstructure reflections (in Fig. 3 a (010) reflection appears near $2\Theta=20°$ and indicates the doubling of the body centered orthorhombic cell below 83 K). In both low temperature phases the CN^- ions point along the former $\langle 110\rangle$ directions of the cubic high temperature phase. These observations confirm the earlier reports of Parry [57] and Rowe et al. [21, 22]. The elastic phase transition in KCN at 168 K is of first order and the cell volume is compressed by approximately 0.3%. At the same time the elastic order in KCN causes large shear distortions of the cubic high temperature cell reaching $\alpha=10.6°$ at 151 K and $\alpha=12.9°$ at 5 K, where α characterizes the reduction of one of the 90° angles of the cubic phase.

The electric ordering removes the disorder of the CN^- molecules with respect to C and N. It is a second-order phase transition, which is illustrated by the temperature dependence of the intensity of the (010) reflection (Fig. 4). The temperature dependence of the structure factor of this superstructure reflection is proportional to the antiferroelectric sublattice polarization and can roughly be described by a spin-1/2 Brillouin function. The result of the calculation is shown as solid line in Fig. 4.

$x=0.85$: for the concentration $x=0.85$ which has hitherto not been investigated the low temperature stable state is a monoclinic phase (Cc) which remains dipolar disordered down to the lowest temperatures (Fig. 5). Similar results were reported for $x=0.8$ by Rowe, Rush and Susman [22]. $(KBr)_{0.15}(KCN)_{0.85}$ exhibits a cubic to monoclinic phase transition at $T=133$ K. In the monoclinic phase the CN^- dumb-

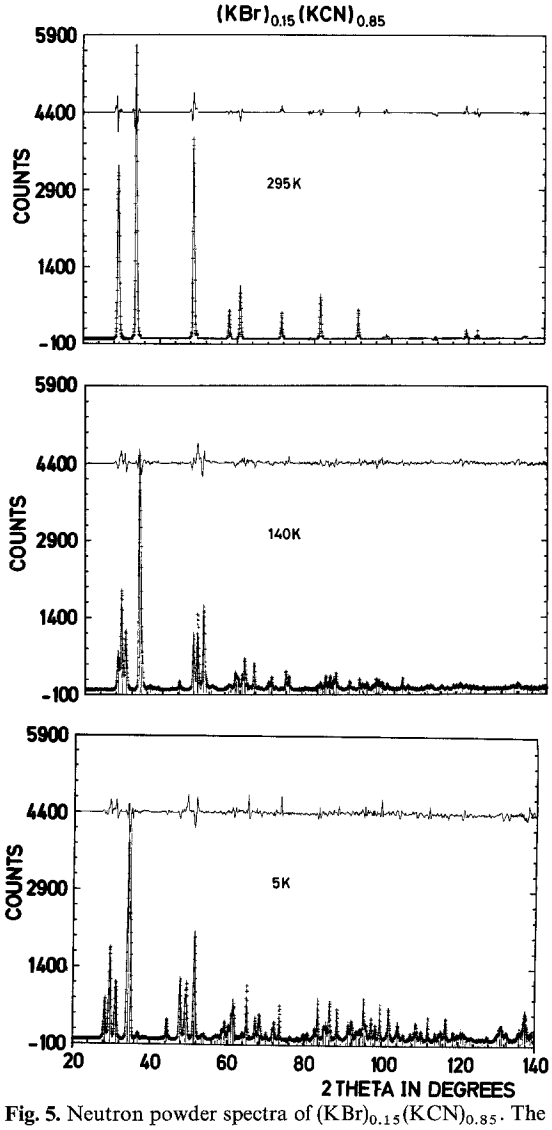

Fig. 5. Neutron powder spectra of $(KBr)_{0.15}(KCN)_{0.85}$. The continuous lines are the best fits of a Rietveld structural refinement. The difference spectra between the best fist and the data points are also shown

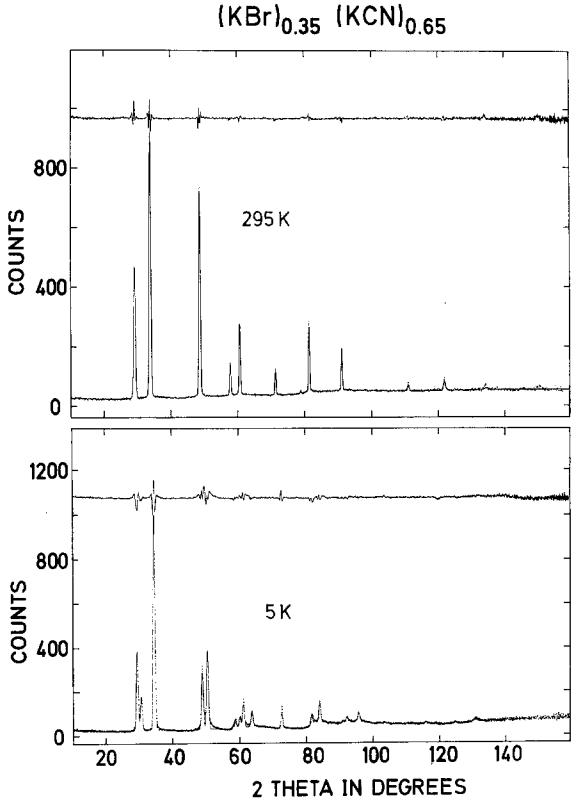

Fig. 6. Neutron powder spectra of $(KBr)_{0.35}(KCN)_{0.65}$ at different temperatures. The continuous lines are the best fits of a Rietveld structural refinement. The difference spectra between the best fits and the data points are also shown

bells point 37.6° off the cubic ⟨111⟩ directions and form an elastic order that is reminescent to a herringbone structure with a modulation vector which corresponds to the L-point of the former cubic Brillouin zone (thus strictly speaking the monoclinic phase is an antiferrodistortive rather than a ferroelastic variety of the cubic phase which appears because of the softening of a coupled translational-rotational mode at the zone boundary). The compression of the volume at the structural phase transition is of the order of 0.4%. The shear distortions with respect to the cubic cell are $\alpha = 0.2°$ and $\beta = \gamma = 5.7°$ at 5 K. It is difficult to answer the question why dipolar order is suppressed in the monoclinic phase, but is observed in the orthorhombic structure. Obviously the elastic order in pure KCN with sheets of ferroelastically ordered molecules favour a dipolar ordering process. This seems not to be the case for $(KBr)_{1-x}(KCN)_x$ crystals that exhibit a herringbone structure. Of course, 180° jumps within the monoclinic cell are still possible. But apparently the hindering barriers for dipolar reorientations are too high and the (virtual) electric phase transition temperature is too low that electric order can occur on a normal experimental time scale.

$x = 0.65$: in this concentration range measurements have been reported previously for concentrations $x = 0.7$ [26] exhibiting a coexistence of monoclinic and rhombohedral low temperature phases and for $x = 0.69$ [27] where a single monoclinic phase has been observed at low temperatures. Significantly we observed a phase transition in $(KBr)_{0.35}(KCN)_{0.65}$ from a cubic plastic phase into a single rhombohedral low temperature phase at 97.5 K. This rhombohedral phase is characterized by one short and three long body diagonals which can easily be recognized by the splitting of the (111)-reflection into two peaks with an intensity ratio of 3:1 with the stronger peak appearing at lower scattering angles (Fig. 6). Usually,

in cubic to rhombohedral ferroelastic phase transitions the cubic cell is elongated along one body diagonal with the molecules oriented along this direction. This kind of behaviour is found at the ferroelastic phase transition of pure CsCN [61]. In the $x=0.65$ sample we find the interesting case of an only partly orientationally ordered crystal where quadrupolar relaxations between the three body diagonals are still possible. As this mixed molecular crystal exhibits no further structural phase transitions down to the lowest temperatures residual entropy exists as T approaches zero and might explain the glassy behaviour of this elastically ordered phase [39]. The strong diffuse scattered intensities that appear near the Bragg reflections at low temperatures are an indication for the more pronounced freezing-in of random shear strains at low temperatures. Equivalently this freezing-in of random strains can be interpreted as a static Debye-Waller factor. At 5 K the Debye-Waller factors in this sample are larger than in pure KCN. This becomes obvious by the fact that no Bragg reflections can be detected in $(KBr)_{0.35}(KCN)_{0.65}$ at scattering angles $2\Theta \geqq 100°$ and for low temperatures.

$x=0.41$ and $x=0.2$: These two concentrations stay cubic down to the lowest temperatures. In Fig. 7 the results are shown for $x=0.41$ at 295 K, 100 K and at 5 K. Inspection of the diffraction profiles of the 41% crystal (Fig. 7) indicates that the Debye-Waller factors increase towards low temperatures and are anomalous large at 5 K. This anomaly in the temperature dependence of the Debye-Waller factors indicates the transition into a low temperature glass state with frozen-in lattice strains and frozen-in orientational correlations.

These neutron diffraction data in combination with previously published diffraction and specific heat data yield a complete phase diagram of $(KBr)_{1-x}(KCN)_x$. The result is shown in Fig. 8. With increasing CN^- concentration x we pass through the sequence cubic/glass-rhombohedral-monoclinic-orthorhombic. For the concentrations studied in this work we could not detect any traces of the triclinic low-temperature phases that have been reported by Knorr and Loidl [23] for $x=0.9$ and by Rowe et al. [25] for $x=0.95$. Specifically we believe that the rhombohedral phase is a well defined state of the virgin crystal and not induced by cycling due to macroscopic strains in the sample. Support to this view is given by a number of cycling experiments on large single crystals utilizing specific heat and neutron diffraction techniques, where we were unable to detect a shift of the transition temperature or to induce traces of low temperature phases other than rhombohedral.

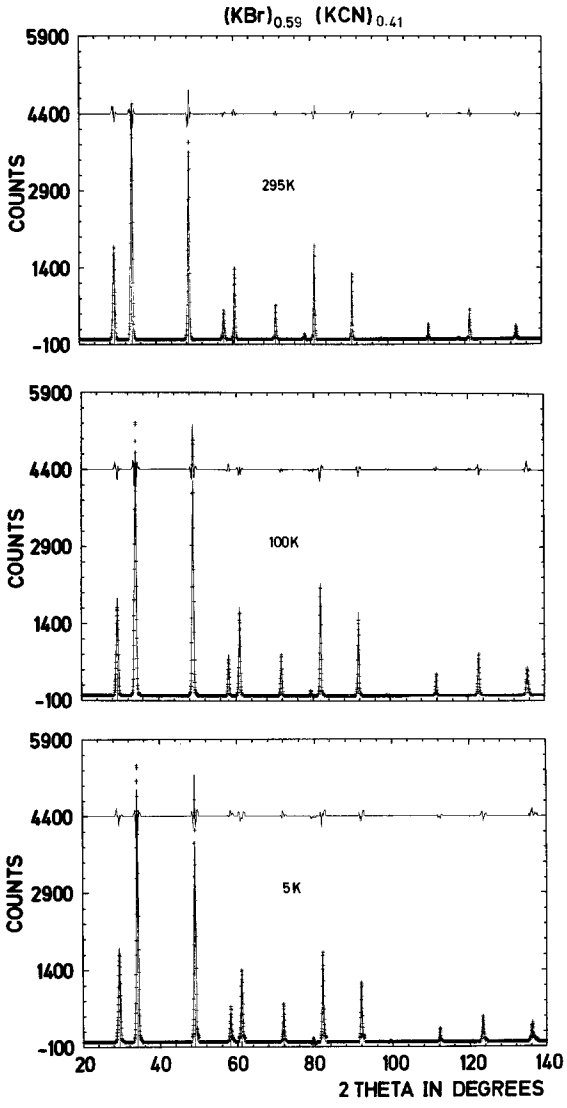

Fig. 7. Neutron powder spectra of $(KBr)_{0.59}(KCN)_{0.41}$ at different temperatures. The continuous lines are the best fits of a Rietveld structural refinement. The difference spectra between the best fits and the data points are also shown

Finally Table 1 gives a summary of the most relevant parameters as determined from the Rietveld refinement in the crystals investigated. The higher resolution of our data compared to earlier studies allows a greater significance to be attached to the refined parameters. In particular the isolation of a single rhombohedral phase for $x=0.65$ permits a more accurate determination of the structure than for the mixed phase of Bouillot et al. [26].

To study the strain-rotation coupling and the rotation-translation coupling in more detail and to determine the degree of frozen-in disorder in the elastically ordered phases and in the glass state we determined the temperature dependence of the Debye-Waller factors for all the concentrations investigated.

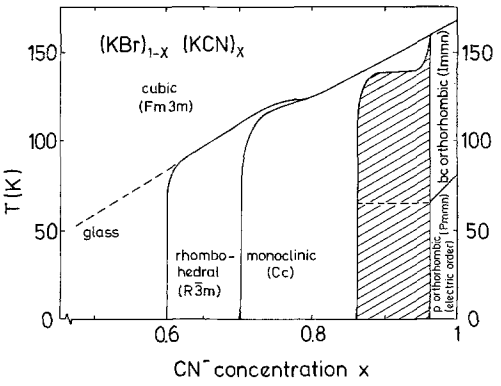

Fig. 8. $x-T$ phase diagram of $(KBr)_{1-x}(KCN)_x$. The solid lines give an estimate of the phase boundaries between different crystallographic phases. The hatched area indicates a broad coexistance region between the monoclinic and the orthorhombic phases. The broken line indicates the transition temperature into the glass state. This line is a continuation of the cubic to rhombohedral phase boundary. Its slope is determined by the anomaly in the quasielastic intensities as detected in the $x=0.57$ crystal at 75 K

Figure 9 shows the temperature dependence of the Debye-Waller factors for the potassium ions $B_K = 8\pi\langle u_i^2\rangle$ for crystals with concentrations $x=1$, 0.85 and 0.41. Here, the $\langle u_i^2\rangle$ are the mean square displacements. Pure KCN and $(KBr)_{0.15}(KCN)_{0.85}$ undergo structural phase transitions which are driven by a strong rotation-translation coupling in T_{2g} symmetry. This transitions involve a softening of the elastic shear constant c_{44} inducing spontaneous shear distortions within a two dimensional subspace of the cubic lattice. A consequence of the softening of T_{2g} phonons is the divergence of the mean square displacements at the transition temperature [18, 62]. The increase of B_K towards the phase transition temperatures can be related to this phenomenon. In pure KCN the structural phase transition is strongly of first order and the softening of the elastic constant c_{44} is by no means complete [13]. Hence, we find no real divergence of the Debye-Waller factors. In $(KBr)_{0.15}(KCN)_{0.85}$ the more pronounced increase of B_K as the transition temperature is approached shows that the 85% crystal is closer to a second-order phase transition. The observation that an increasing Br^- substitution in KBr:KCN drives the phase transitions closer to second order is in agreement with the results of [16] where an almost continuous phase transition has been reported for a crystal with a CN^- concentration $x=0.73$. For $x=0.41$ the Debye-Waller factors pass through a minimum and increase again with decreasing temperatures. Again this anomalous behaviour signals that dynamic disorder is introduced by the long wavelength fluctuations which appear close to a structural phase transition. However, for $x=0.41$ the phase transition into an orientationally ordered state is suppressed and these fluctuations are frozen-in yielding a highly enhanced static Debye-Waller factor at low temperatures. This behaviour can be viewed as a fingerprint of the glass state in the alkali halide-alkali cyanide mixtures.

A further interesting insight into the statics and the dynamics of these molecular crystals can be gained by examining the concentration dependence of the Debye-Waller factors as measured at 295 K and at 5 K. The results are given in Fig. 10, where the Debye-Waller factors are plotted versus the concentration x. The mean square displacements of the Br^-/CN^- ions exhibit qualitatively a very similar concentration dependence. At room temperature the Debye-Waller factors steadily decrease with decreasing concentration reaching a finite value at low x. This curve is a measure of the disorder of the plastic phase which is introduced by the fast reorientations of the CN^- molecules. At low temperatures the x-dependence of the mean square displacements behaves quite different. $B_K(x)$ decreases for $x\to 0$ and $x\to 1$ and exhibits a maximum near the critical concentration. The increase at medium concentrations is a measure of the frozen-in disorder due to the impurity centers yielding a static Debye-Waller factor. The asymmetry of the curve can be explained by the fact that the concentration dependence of the strength of the random fields $x\cdot(1-x)$, which is introduced by the impurity ions, is weighted with the rotation-translation coupling constant which increases linearly with x. Thus the concentration dependence of the Debye-Waller factors at low temperatures can be described by $x^2\cdot(1-x)$, which is plotted as solid line in Fig. 10. A similar concentration dependence of the dynamic structure factor of the orientational motion was predicted by K.H. Michel [37]. This behaviour gives direct evidence that fluctuations of shear strains coupled to orientational correlations are frozen-in by the static random strains. Near the critical concentration, where the elastic constant c_{44} is almost zero, and thus where the lattice is close to a two-dimensional melting instability, critical fluctuations are pinned and a maximum in the frozen-in disorder becomes apparent. For lower concentrations the random strains dominate and weaken the rotation-translation coupling considerably. Hence the freezing-in of the orientational degrees of freedom is driven by the coupling to the random field and becomes more and more a single ion phenomenon. For higher concentrations the rotation-translation coupling drives the structural instability and establishes a low temperature phase with a long range ordered homogeneous shear distortion.

Table 1. Structural parameters for $(KBr)_{1-x}(KCN)_x$ as determined by Rietveld refinement techniques for concentrations $x=1$, 0.85, 0.65, 0.41 and 0.2 at various temperatures. Lattice parameters: a, b, c, α, β and γ; volume of the unit cell: V; atomic positions for the K and the CN/Br ions: x, y, z; distortions with respect to the cubic cell: $\Delta\alpha$, $\Delta\beta$, $\Delta\gamma$; the new cell parameters with respect to the cubic cell are thus: $90°+\Delta\alpha$, $90°+\Delta\beta$ and $90°+\Delta\gamma$; CN^- bond length: l; nuclear R-factor for the Bragg peaks only: R_{nuc}

conc. x	T[K]	structure	cell parameter							atomic positions in units of a, b, c							$\Delta\alpha, \Delta\beta, \Delta\gamma$ [deg]	l[Å]	R_{nuc}
			a[Å]	b[Å]	c[Å]	α	β	γ [deg]	V[Å]^3	x	y	z	x	y	z				
1	290	fc cubic Fm3m	6.523	–	–	–	90	–	277.6	0	0	0 (K)	0.5	0.5	0	(CN/Br)	0		4.9
	151	bc ortho Immm	4.268	5.141	6.183	–	90	–	135.7	0	0	0 (K)	0.5	0.5	0	(Br)	−10.6	1.121	8.6
													0.5	0.609	0	(CN/2)	0		
													0.5	0.391	0	(CN/2)	0		
	5	p ortho Pmnm	4.192	5.257	6.083	–	90	–	134.1	0.273	0	0 (K)	0.5	0.750	0	(Br)	−12.86	1.157	6.9
													0.5	0.860	0	(C)	0		
													0.5	0.640	0	(N)	0		
0.85	290	fc cubic Fm3m	6.539	–	–	–	90	–	279.6	0	0	0 (K)	0.5	0.5	0	(CN/Br)	0		5.4
	132	monoclinic Cc	7.649	4.603	9.196	90	90	122.76	272.3	0	0.029	0 (K)	0.539	0.002	0.265	(Br)	−0.06		13.6
													0.497	0.071	0.214	(CN/2)	−2.90		
													0.580	−0.067	0.317	(CN/2)	−2.90		
	5	monoclinic Cc	7.508	4.605	9.185	90	90	121.77	270.0	0	0.039	0 (K)	0.489	−0.013	0.237	(Br)	−0.14	1.166	11.4
													0.454	0.075	0.183	(CN/2)	−4.09		
													0.526	−0.100	0.291	(CN/2)	−4.09		
0.65	295	fc cubic Fm3m	6.546	–	–	–	90	–	280.6	0	0	0 (K)	0.5	0.5	0	(CN/Br)	0	1.158	3.07
	5	rhomb $R\bar{3}m$	4.509	–	–	–	61.94	–	270.5	0	0	0 (K)	0.096	0	0.5	(CN/Br)	+1.65	–	12.97
																	+1.65	–	
																	+1.65	–	
0.5	292	fc cubic Fm3m	6.574	–	–	–	90	–	284.2	0	0	0 (K)	0.5	0.5	0	(CN/Br)	0	–	2.3
0.2	292	fc cubic Fm3m	6.593	–	–	–	90	–	286.6	0	0	0 (K)	0.5	0.5	0	(CN/Br)	0	–	7.5

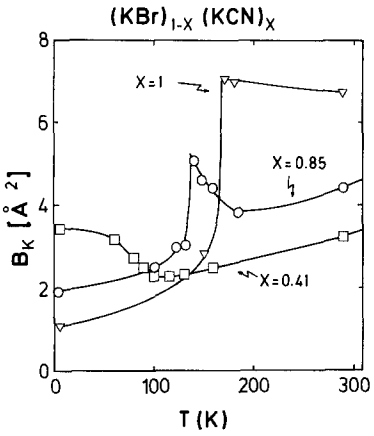

Fig. 9. Temperature dependence of the Debye-Waller factors of the K^+ ions in $(KBr)_{1-x}(KCN)_x$ for concentrations $x=1$ (▽), 0.85 (○) and 0.41 (□). The solid lines are drawn to guide the eye

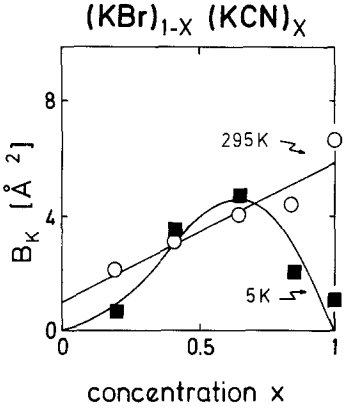

Fig. 10. Concentration dependence of the Debye-Waller factors of the K^+ ions in KBr:KCN mixed crystals at 295 K (○) and at 5 K (■). The solid lines were calculated as described in the text

B. Single crystal diffraction

For a detailed analysis of the frozen-in strains and the frozen-in orientational correlations we performed a single crystal diffraction study in $(KBr)_{1-x}(KCN)_x$. Some results of these investigations have been published previously [34, 35]. These experiments were carried out on the triple axis spectrometer D 10 located on a thermal neutron guide at the Insitut Laue-Langevin. The samples were mounted on an Eulerian cradle to allow scanning along all lattice directions. A vertical focusing (200) Cu-monochromator gave a wave length of 1.26 Å. A pyrolytic graphite analyzer was set to the (004) reflection to give an energy resolution of approximately 1.5 meV and was set to zero energy transfer. A He-flow cryostat [63] allowed variation of the temperature from 10 K to 300 K with an accuracy of 0.1 K.

In the present article we pay special attention to the question of the extent to which the freezing-in of the orientational degrees of freedom is a cooperative phenomenon. The following ideas are based on the recent theory by K.H. Michel [37, 38]: In this theory the role of random strain fields is twofold: *i*) they couple linearly to the orientational order parameter [37] and *ii*) through anharmonic coupling with the dynamic modes, the static strains lead to a scattering of these dynamic modes and therefore to internal friction [38]. Friction processes become dominant if the restoring forces are weak. The latter conditions however imply that the collective interactions which drive the system towards a structural phase transition (soft mode) are strong in comparison to the pure random field effect *i*). One is led to distinguish two situations: In the first place in strong random fields, the structural phase transition is simply suppressed by *i*) and orientations and strains freeze in continuously. And secondly in weak random fields processes *ii*) can cause a nonergodic instability. Notice however that the condition of weak random fields is not sufficient. In addition one needs the neighbourhood of a second order phase transition. If the system undergoes a first order transition, the nonergodic instability does not occur as a dynamic phenomenon.

To decide whether the glass transition in the cyanide glasses is a nonergodic instability or if the freezing-in of the orientational degrees of freedom is dominated by strong random fields the temperature dependence of the order parameter has to be studied. A nonergodic instability gives a sudden increase of the diffuse elastic intensities at the glass transition [38], while strong random field systems exhibit a smooth T^{-2} dependence with no discontinuities [37]. Of course, in the case of weak random fields one can have a superposition of two effects: continuous freezing processes at high T and a nonergodic instability at the glass transition.

To clarify the situation in KBr:KCN experimentally we performed a single crystal diffraction study for concentrations just above and just below the critical concentration. In the Figs. 11 and 12 we show transverse scans through the (060) reflection in mixed crystals with concentrations $x=0.65$ and $x=0.57$ at various temperatures. The profiles can be described by a resolution-limited Bragg scattering (empty Gaussian area) and by an exponentially decaying diffuse contribution (shaded area) [35, 36]. The exponential line shape was described by $I=I_0\cdot\exp(-\sigma q)$ where q is the phonon wave number and the coefficient σ determines the width of the line. For both crystals we find a large increase of the diffuse scattered intensi-

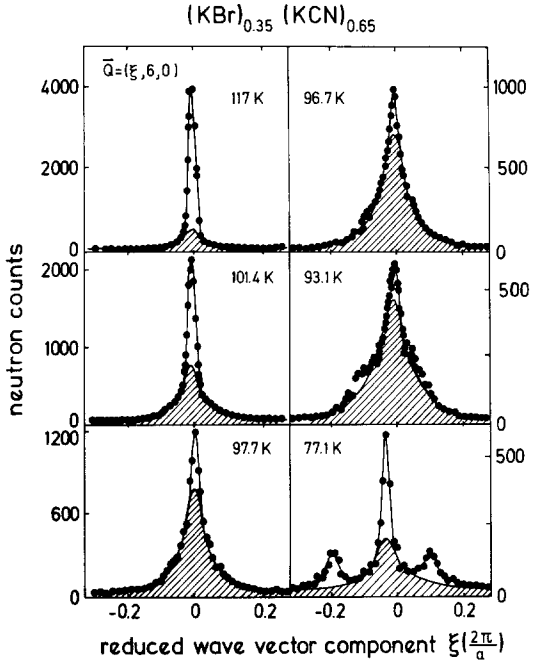

Fig. 11. Transverse scans at zero energy transfer through the (060) reflection in $(KBr)_{0.35}(KCN)_{0.65}$ at various temperatures. The cubic to orthorhombic phase transition temperature at 97.5 K has been determined calorimetrically by Mertz and Loidl (Ref. 28). The shaded area shows the contribution from frozen-in shear strains, the empty area that from Bragg scattering; the solid lines represent the result of fits as explained in the text. (Figure taken from Ref. 35 and reproduced with permission by courtesy of The American Physical Society)

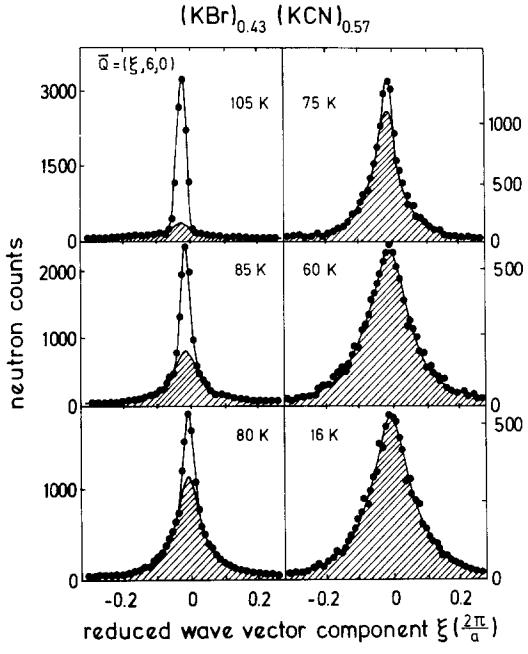

Fig. 12. Transverse scans at zero energy transfer through the (060) reflection in the (001) plane of $(KBr)_{0.43}(KCN)_{0.57}$ at various temperatures. The hatched area shows the diffusive contribution from frozen-in strain fields, the empty peak the "true" Bragg intensity. The solid lines are the results of fits as described in the text. (Figure taken from Ref. 35 and reproduced with permission by courtesy of The American Physical Society)

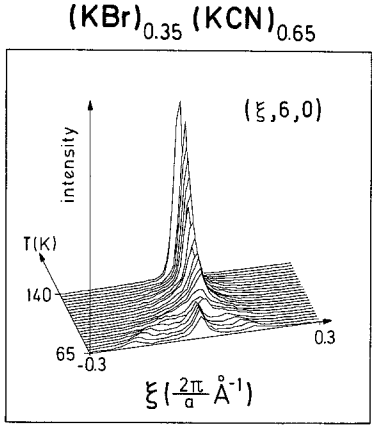

Fig. 13. Three-dimensional plots of the line shapes of transverse scans through the (060) reflection in $(KBr)_{0.35}(KCN)_{0.65}$. The intensities are shown versus the reduced wave vector component for a series of temperatures between 65 K and 140 K

ties for temperatures $T<100$ K and at the same time a strong decrease of the Bragg scattering contributions. It demonstrates how the freezing-in of molecular orientations which are coupled to long-wavelength transverse phonons influences the static properties: in both crystals the Bragg intensities go almost to zero which indicates the strong increase of the Debye-Waller factors with decreasing temperatures. The diffuse scattered intensities can be explained by frozen-in local shear distortions (transverse phonons with zero energy). Obviously the freezing of coupled orientational and translational modes decreases the intensity of the Bragg reflections and increases at the same time the diffuse intensities around the reciprocal lattice points. $(KBr)_{0.35}(KCN)_{0.65}$ undergoes a phase transition at 97.5 K. Below this temperature the "static" local shear deformations become partially removed by one uniform rhombohedral distortion. However, even well below the phase transition frozen-in strain fields can still be detected. In $(KBr)_{0.43}(KCN)_{0.57}$ no long range orientational order is established and the critical fluctuations are frozen-in. On the average this crystal stays cubic down to the lowest temperatures with local distortions appearing for $T<100$ K. Below 60 K the diffraction patterns are almost temperature independent. At this temperature the freezing process is completed and the glassy state is fully established.

The close analogy between the phase transition in $(KBr)_{0.35}(KCN)_{0.65}$ and the glass transition for the $x=0.57$ crystal is nicely demonstrated in the Figs. 13

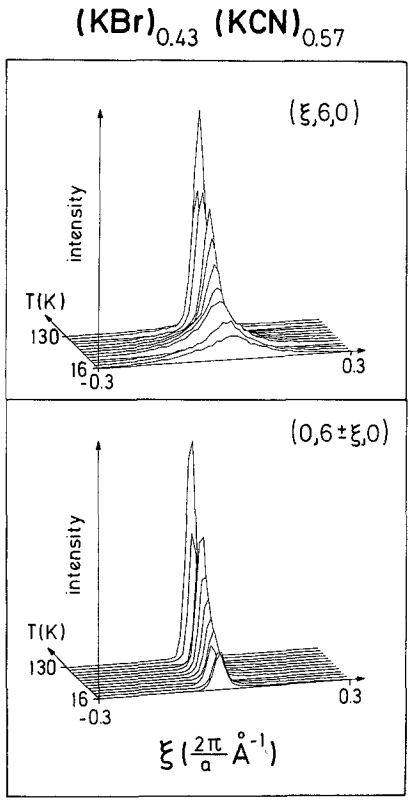

Fig. 14. Three dimensional plots of the line shapes of transverse and longitudinal scans through the (060) reflection in the (001) plane of $(KBr)_{0.43}(KCN)_{0.57}$. The intensities are shown versus the reduced wave vector component ξ for a series of temperatures between 16 K and 130 K:
upper part: transverse scans along $(\xi, 6, 0)$
lower part: longitudinal scans along $(0, 6 \pm \xi, 0)$

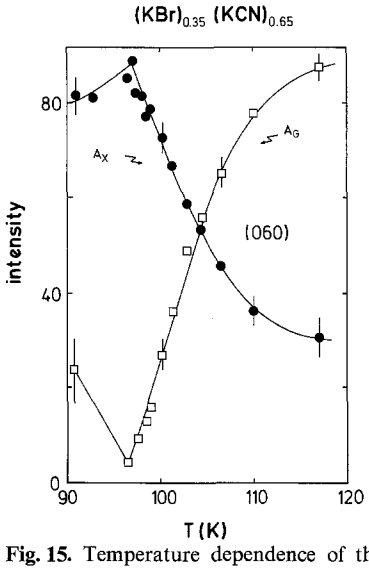

Fig. 15. Temperature dependence of the intensities of the Bragg peaks (Gaussian area: A_G (□)) and of the quasielastic lines (area as defined by the exponential line shape: A_X (●)) as measured at the (060) reciprocal lattice point in the mixed crystal with a concentration $x = 0.65$. The lines are drawn to guide the eye

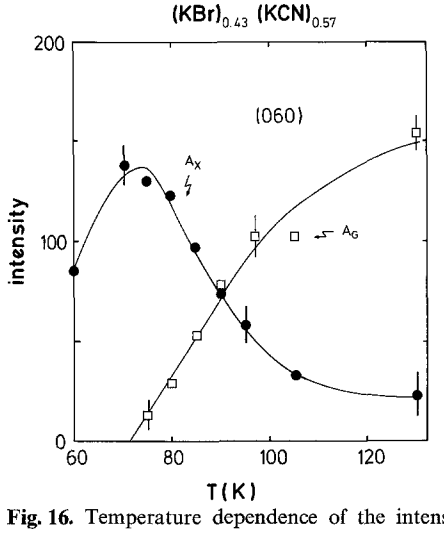

Fig. 16. Temperature dependence of the intensities of the Bragg peaks A_G (□) and of the quasielastic lines A_X (●) as determined at the (060) reciprocal lattice point in $(KBr)_{0.43}(KCN)_{0.57}$. The lines are drawn to guide the eye

and 14. Figure 13 shows the temperature variation of the scattered intensity in transverse scans along $(\xi 60)$. The splitting of the (060) Bragg peak indicates the cubic to rhombohedral phase transition (the peak in between the two outer rhombohedral peaks is due to the two poorly resolved out-of-plane rhombohedral peaks). The upper part of Fig. 14 shows the equivalent temperature dependent plot for $x = 0.57$. This figure gives a clear impression of the break-down of true long-range order in this crystal. The observed line shapes can be interpreted as a distribution of static T_{2g} shear distortions centered around the undistorted lattice. Despite the absence of Bragg scattered intensities in transverse scans, the longitudinal scans (lattice constant scans) yield well defined "Bragg peaks" (Fig. 14, lower part). However, the temperature dependence of the intensities is highly anomalous.

Quantitative results of the temperature dependence of the intensities of the Bragg peaks and of the quasielastic intensities at the (060) reciprocal lattice point for the crystals with concentrations $x = 0.65$ and $x = 0.57$ are shown in the Figs. 15 and 16. With decreasing temperatures in the 65% crystal the intensity of the Gaussian peaks (Gaussian area: A_G) decreases, passes through a minimum at the phase transition temperature and increases again for further decreasing T. In the rhombohedral phase we integrated the intensities of the 4 rhombohedral Bragg peaks due to the multi-domain structure. The diffuse scattered intensities (exponential area: A_X) strongly increase

for $T<110$ K and exhibit a maximum at the structural phase transition temperature. To determine the diffuse scattered intensities in the rhombohedral phase we fitted only one exponential line shape to the peak profile as can be seen in Fig. 11. For the crystal with a concentration $x=0.57$ the Bragg intensities vanish at $T\approx 70$ K. Astonishingly, also in this glassy crystal the diffuse scattered intensities exhibit a maximum near 75 K.

In discussing the results as presented in the Figs. 15 and 16 three characteristic features have to be noted: *i*) the highly anomalous Debye-Waller factors, which increase with decreasing temperatures; *ii*) the increase of the diffuse scattered intensities which is much stronger than $1/T^2$ as expected for strong random fields and *iii*) a maximum in the diffuse scattered intensities as well in the ordering as in the glassy compounds. Points *i*) and *ii*) are strongly correlated: of course the freezing-in of shear strains enhances the "static" Debye-Waller factors. The deviations in the T^{-2} dependence could in principle be explained by the fact, that A_X includes intensities of thermal fluctuations and of critical scattering. This can be true for the crystal that undergoes a structural phase transition. However, the minimum in c_{44} for $x=0.57$ we expected near $T\approx 95$ K (the minimum c_{44} for $x=0.5$ was detected near 90 K by Rowe et al. [2] and the structural phase transition in the crystal with $x=0.65$ occurs at $T=97.5$ K) where the diffuse intensities increase most strongly. Thus we believe that the increase of A_X in $(KBr)_{0.43}(KCN)_{0.57}$ is a fingerprint of a nonergodic instability. The maximum in the temperature dependence of the diffuse intensities A_X is due to the onset of long range elastic order in the 65% crystal, while for $x=0.57$ an interpretation in terms of a residual quadrupolar ordering process within (or between) the clusters seems to be straight forward. A more detailed investigation and discussion of this low-temperature anomaly will be given below.

To show that the local shear distortions are of T_{2g} symmetry we plotted in Fig. 17 the intensity contour lines of the diffuse scattered intensities around the (020) and the (440) reflections for $x=0.65$ just above the structural phase transition. Very similar results were obtained for the 57% crystal at low temperatures and analogous data have been published by Rowe et al. [2] and by Loidl et al. [34] in crystals below the critical concentration. These contour lines follow exactly the dynamic structure factor of transverse phonons with a sound velocity proportional to c_{44}. Two facts appear to be important: *i*) the contour lines exhibit an extreme anisotropy and *ii*) the $(hh0)$ reflections show in addition an asymmetry along the cube axis. Point *i*) explains the fact that in longitudinal scans the diffuse scattered intensities are rather small

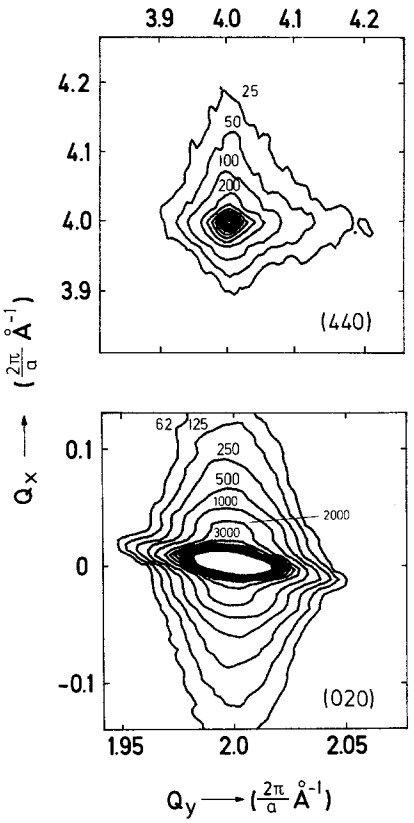

Fig. 17. Equal intensity contour lines around the (020) and the (440) reciprocal lattice point in the $x=0.65$ crystal just above the structural phase transition at 97.7 K:
upper part: equal intensity contour map at the (440) reflection. The maximum peak intensity was 980 counts.
lower part: equal intensity contour map at the (020) reflection. Here the maximum peak intensity was 15500 counts

and that in powder diffraction experiments the line broadening is much less apparent. The asymmetry can be explained by the bilinear coupling of rotations and translations [15]. To study this effect in more detail we followed the temperature variation of scans along the $(0\xi 0)$ direction through the (440) reflection. A representative result is shown in Fig. 18. At 16 K a small Bragg spike appears on top of a broad diffuse component that exhibits a distinct asymmetry. The result of a fit to the scan profile including symmetric and asymmetric contributions is indicated by the solid line. The diffuse intensities were fitted using exponential line shapes [35, 36]. The separation of the total intensity into symmetric and asymmetric contributions is indicated in the lower part of Fig. 18. The line width of the asymmetric part is much wider than that of the symmetric part (theoretically the symmetric part should follow a $1/q^2$ dependence, while the asymmetric part of the diffuse scattered intensities should go like $1/q$ [17]. Experimentally, symmetric and asymmetric contributions follow exponential line

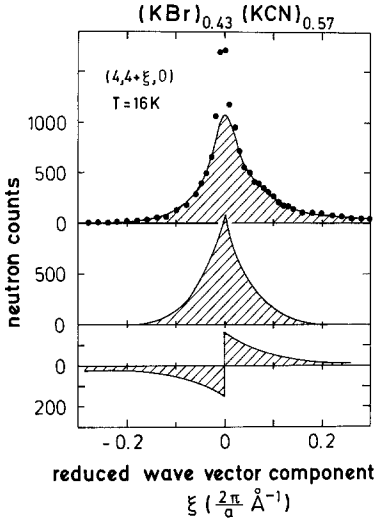

Fig. 18. Transverse scans through the (440) reciprocal lattice point in $(KBr)_{0.43}(KCN)_{0.57}$. The shaded area gives the total diffuse intensities as determined by fits to the data points. In the lower parts of the figure the deconvolution of the diffuse scattered neutron intensities into symmetric and into antisymmetric contributions are shown

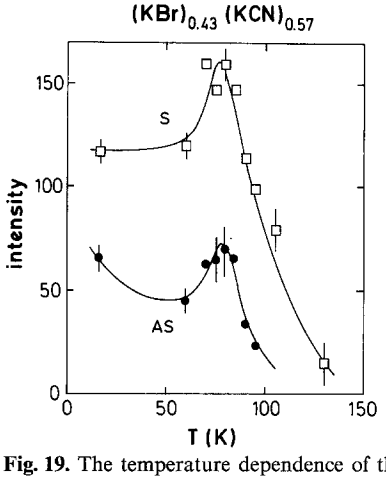

Fig. 19. The temperature dependence of the intensities of the symmetric (S: □) and of the antisymmetric (AS: ●) components of the diffuse intensities as measured at the (440) reciprocal lattice point in the $x=0.57$ crystal. The lines are drawn to guide the eye

shapes with the coefficient σ of the asymmetric contributions being a factor of two larger than that of the symmetric contributions.

The temperature dependence of the areas of the symmetric and asymmetric component of the diffuse intensities as measured at the (440) reciprocal lattice point for $x=0.57$ is given in Fig. 19. Both intensities start to increase suddenly at about 110 K exhibiting a similar temperature dependence as that measured at the (060) reciprocal lattice point (Fig. 16). At all

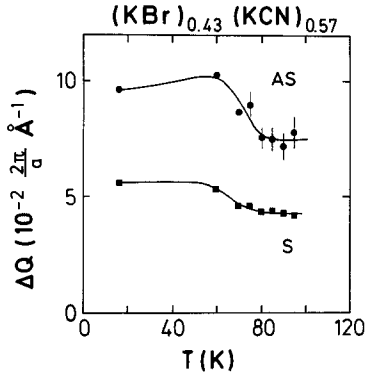

Fig. 20. Half width at half maximum in momentum space ΔQ of the diffuse scattered intensities versus temperature in $(KBr)_{0.43}(KCN)_{0.57}$. The width of the symmetric (S: ■) and of the antisymmetric component (AS: ●) are shown separately. The lines are drawn to guide the eye

temperatures the areas of symmetric contributions are roughly twice as large. Again, as mentioned before, the sudden increase and the temperature-dependence, that is much stronger than T^{-2}, point towards a non-ergodic instability. Also in the temperature dependence of the diffuse intensities, as measured at the (440) reflection, there appears a further anomaly in both components at 75 K and the intensities exhibit a sudden decrease reaching a constant value at temperatures below 50 K. These effects have never been detected by measuring the intensities of the central line in inelastic experiments. The central peak intensity is given by the area of energy scans through the diffuse intensities and measures the temperature dependence of the diffuse scattered intensities at a certain q-value. This disagreement can be explained by studying the temperature dependence of the line width ΔQ of the diffuse intensities. The results are given in Fig. 20. At temperatures $T>75$ K the line widths stay constant but increase towards lower temperatures. Obviously the line broadening effect corresponds to the decrease of the intensities. In Fig. 21 this phenomenon is studied in more detail for the $(0k0)$ reflections where we show the Q-dependence of the line broadening for a series of measurements at different reciprocal lattice points. At temperatures $T>75$ K the line widths ΔQ strictly follow a linear Q-dependence, a behaviour that can be explained in terms of an inhomogeneous strain broadening. However, for lower temperatures significant deviations become apparent with a strong increase of the line width for higher Q-values. The temperature dependence of the line widths of the (060) and (080) reflections are shown as an inset. Until now central peak intensities have only been measured near the (111), (200) and (220) reflections. The line widths ΔQ of the diffuse intensities at these values of momentum transfer stay

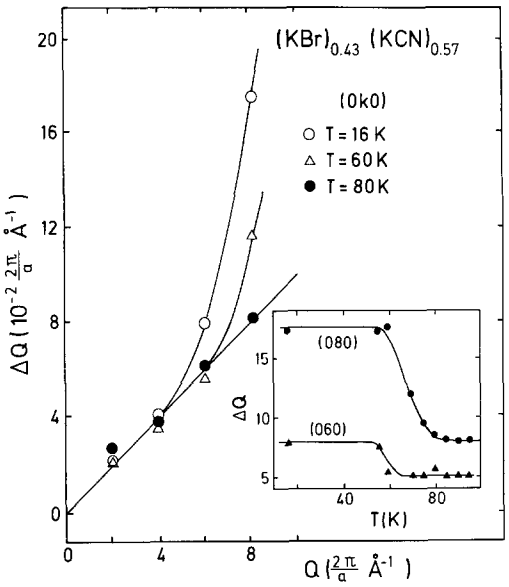

Fig. 21. Half width at half maximum ΔQ of the diffuse scattered intensities versus momentum transfer at different temperatures as measured in $(KBr)_{0.43}(KCN)_{0.57}$. Note the strong deviations from a linear Q-dependence as expected for a broadening due to random strains for temperatures $T \leqq 75$ K. The inset shows the temperature dependence of ΔQ for the (060) and the (080) reflections. The lines are drawn to guide the eye only. (Figure taken from Ref. 35 and reproduced with permission by courtesy of The American Physical Society)

roughly constant at all temperatures and no anomalies in the intensities can be detected. At higher Q values and lower temperatures an additional broadening becomes apparent. In addition, this broadening seems to be rather isotropic giving lower intensities in transverse scans. We believe that the anomalies at 75 K are due to quadrupolar interaction effects. If we extrapolate the structural phase transition temperature from $x > x_c$ to $x = 0.57$ we find exactly 75 K. Compared to the $x = 0.65$ sample the rotation-translation coupling is already too weak to establish long range orientational order and homogeneous shear deformations of the center of mass lattice. However, we believe that local ordering of CN^- ions, which are exposed to weak random fields only, is responsible for the observed anomalies.

Therefore, in explaining the temperature dependence of the diffuse scattered intensities two different effects have to be taken into account: the increase of the diffuse scattered intensities below 110 K as a result of the slowing down of dynamic shear fluctuations coupled to random strains and quadrupolar ordering processes which give a long range shear deformation for $x = 0.65$ but only short range order for $x = 0.57$. The former process appears above ($x = 0.65$) and below ($x = 0.57$) the critical concentration. $(KBr)_{0.35}(KCN)_{0.65}$ undergoes a structural phase transition at $T = 97.5$ K and the inhomogeneous shear deformations are reduced in favour of the long range rhombohedral distortion. In $(KBr)_{0.43}(KCN)_{0.57}$ the critical fluctuations are frozen-in due to random strains, giving a network of clusters with a distribution of shear deformations. Presumably, the residual quadrupolar ordering process is indicated by anomalies in the temperature dependence of the intensities and the line width of the diffuse scattered intensities.

C. Quasielastic measurements

In the previous two sections we have discussed the structural properties of KBr:KCN crystals in some detail. We found a strong increase of diffuse scattered intensities near reciprocal lattice points which become frozen-in in the glass state. In the cyanide glasses static random strain fields play an essential role [37]. They couple to the orientational order parameter and can explain in part these diffuse intensities. However, it seems that the sudden increase and the strong temperature dependence of the central peak phenomenon point towards a nonergodic instability [38]. At the glass transition the crystals are close to a second-order ferroelastic phase transition and the long-wavelength acoustic phonons are extremely soft. The structural relaxations connected with the long-wavelength lattice deformations slow down and are finally arrested in the glass state: the local shear deformations are trapped by the static random potentials. The glass transition can be interpreted as a localization of phonon modes [38] and below the glass transition the system is characterized by zero-energy frozen-in phonons.

The aim of this quasielastic neutron scattering investigation was to study the freezing-in of critical fluctuations with time-of-flight techniques in order to detect a finite energy width in the central peak. Utilizing time-of-flight (TOF) techniques high energy resolution can be achieved. However, the momentum resolution is lost due to the use of polycrystalline material and information can be obtained as an average over the Brillouin zone only. The experiments were performed on the TOF spectrometer IN6 located on a cold neutron source at the ILL. Incident neutron energies of 3.15 meV have been used and crystals with concentrations $x = 0.57$ and $x = 0.2$ have been investigated. The energy resolution of the experimental set up was 0.048 meV (half width at half maximum). Additional measurements were performed utilizing the TOF spectrometer IN4 with an incident neutron energy of 12.5 meV. The energy resolution of this set of experiments was 1 meV. These experiments were performed to get a rough estimate of the phonon den-

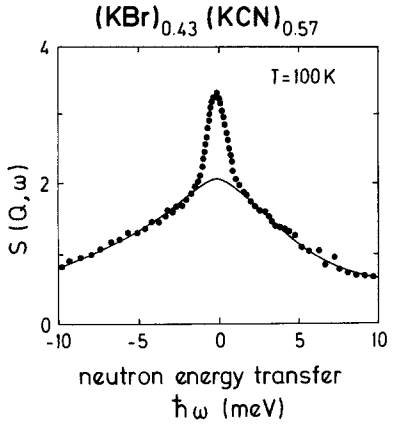

Fig. 22. Dynamic structure factor $S(Q,\omega)$ as measured in $(KBr)_{0.43}(KCN)_{0.57}$ at $T=100$ K. The incident energy was 12.5 meV and the scattering angle was chosen as $2\Theta=75$ deg. corresponding to a Q value of approx. 3 $Å^{-1}$. The solid line is a fit to a single Lorentzian line shape including the detailed balancefactor. The Gaussian peak at zero energy transfer is predominantly determined by elastic incoherent scattering; its width is completely determined by the experimental resolution

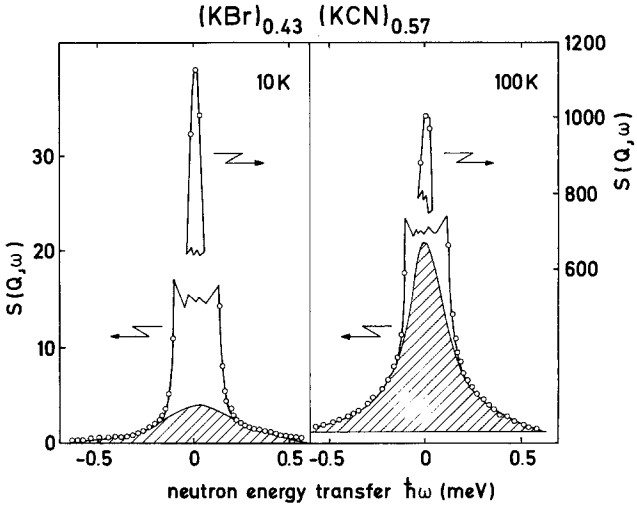

Fig. 23. Dynamic structure factor $S(Q,\omega)$ as measured in $(KBr)_{0.43}(KCN)_{0.57}$ with an incident energy of 3.15 meV at $T=100$ K and at $T=10$ K. Note the different scales for the purely static (resolution limited) and the quasielastic components. The solid lines represent fits to a resolution limited Gaussian and a broader Lorentzian line shape. The shaded area corresponds to critical fluctuations

sity of states in a wider energy window which was necessary to get a measure of the influence of the soft lattice near the structural instability on the dynamic structure factor $S(Q,\omega)$ at low frequencies.

In Fig. 22 we show $S(Q,\omega)$ in $(KBr)_{0.43}(KCN)_{0.57}$ as measured at the IN4 in a frequency window from -10 meV to 10 meV at 100 K. Below the central line at zero energy transfer which is resolution limited and predominantly due to elastic incoherent scattering we find a structureless spectrum that can be described by a Lorentzian line shape with a half width at half maximum of 4 meV. $S(q,w)$ looks like a spectrum of an ensemble of damped oscillators or like a fluid-like spectrum. No fine structure due to zone boundary transverse phonons can be detected. These findings can be explained by the strong rotation-translation coupling which is active in this system. At $T=100$ K the lattice is extremely soft and the damping is high. We take this spectrum as the phonon background. We now focus on much finer energy scales to detect the freezing-in of critical fluctuations.

Figure 23 shows two representative results in $(KBr)_{0.43}(KCN)_{0.57}$ as measured at the IN6 at 10 K and 100 K. These measurements were performed at Q-values close to the (111) reciprocal lattice point. The phonon background at $T=100$ K is indicated as a straight line and represents just the maximum of the Lorentzian line as shown in Fig. 22. At $T=10$ K the phonon contribution is almost negligible due to the thermal population. Already a first inspection clearly demonstrates two features:

– at $T=10$ K we find a significant increase of the purely static component compared to the 100 K data. This static contribution due to the broken ergodicity of the glass state is placed on top of a strong elastic incoherent peak at zero energy transfer and

– in both spectra a narrow quasielastic component can be detected. This quasielastic peak is large and narrow at 100 K and small and considerably wider at $T=10$ K.

We fitted the data using a Gaussian line shape for the resolution limited static part and a Lorentzian line shape for the quasielastic line. The results are shown as solid lines in Fig. 23. Here the hatched areas give the quasielastic peaks. The temperature dependence of the Gaussian and the Lorentzian areas and of the Lorentzian line width as measured in the crystal with a concentration $x=0.57$ is shown in Fig. 24. At present it is not clear where to locate exactly the glass transition temperature in this crystal. Obviously, the upper limit (110 K) is the temperature where the strongest increase of the diffuse intensities becomes apparent; the lower limit (75 K) is the temperature where the anomaly appears in the temperature dependence of the diffuse scattered intensities (Figs. 19–21). Despite these uncertainties, the following overall behaviour is clearly demonstrated: in the plastic phase we find a quasielastic component that increases in intensity and in width as the glass transition is approached. This behaviour characterizes the slowing down of the critical fluctuations. Below the glass transition a purely static component increases while the dynamic component decreases in intensity and increases in width.

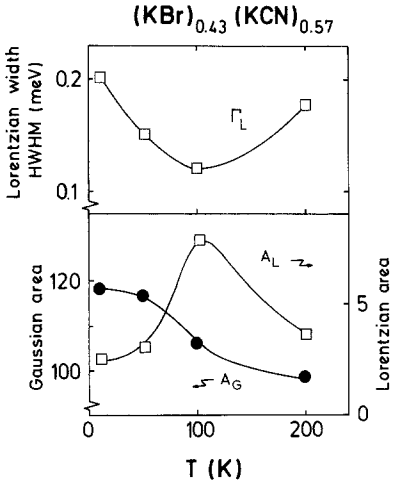

Fig. 24. Temperature dependence of the Lorentzian line width (half width at half maximum (T_L: □); upper part) and of the Gaussian (A_G: ●) and the Lorentzian (A_L: □) intensities. Note the different scales for the Gaussian and the Lorentzian areas and the suppressed zero for the Gaussian component. The lines are drawn to guide the eye only

These findings closely resemble recent dynamic theories and computer simulations of the glass transition in supercooled liquids [64–66]. This is not astonishing, since Michel's model [38] with anharmonic scattering of dynamic modes and random strain fields leads to a simple variant of the mode coupling theories. In the framework of these theories the dynamic structure factor has been calculated. At the glass side a quasielastic peak increases in height and width as the glass transition temperature is approached from below. This quasielastic peak corresponds to dynamical critical fluctuations. In addition a $\delta(\omega)$ peak characterizes the static component of the glass state. At the liquid side of the transition no strictly elastic contribution appears, but a much stronger quasielastic peak which increases in height as the transition temperature is approached from above.

We are aware that the supercooling of a hard sphere model is quite different to the dynamics of the glass transition in KBr:KCN systems. However, in supercooled liquids the cage effect, where an atom is being trapped by its surrounding atoms, plays an important role. The mode coupling theories exhibit this trapping effect as a prominent feature. Analogous, in KBr:KCN shear distortions are pinned by static random fields and contribute via a direct feedback to the freezing dynamics.

At present further time-of-flight experiments are being planned on KBr:KCN crystals with different concentrations, with even better energy resolution and with much finer temperature steps around the glass transition temperatures. With these experiments we hope to test if the striking similarity of our results with the predictions of the mode coupling theories holds for a closer inspection. E.g. mode coupling theories [65] predict a double peak structure in $S(Q, \omega)$ just above the glass transition which characterize the α- and the β-relaxation (structural and secondary relaxation respectively). In KBr:KCN glasses it is known that the structural and the secondary relaxation exhibit a fully decoupled sequential freezing [67, 68] with a well-known relaxational dynamics. It seems worth to investigate the dynamic structure factor close to the glass transition in order to detect the predicted double peak structure.

V. Conclusions

In this article we have reported a series of neutron scattering studies in the mixed molecular system KBr:KCN including powder diffraction, single crystal diffraction and quasielastic neutron scattering techniques. The most relevant results of this detailed investigation can be summarized as follows:

– we presented a detailed phase diagram of KBr:KCN mixtures. Here we analyzed transition temperatures in powder samples and in single crystals and were able to compare directly the results to those as observed in specific heat measurements on large single crystals (Mertz and Loidl, 28). We performed a number of cycling experiments with various heat treatments and annealing times and finally believe that the phase diagram as presented in Fig. 8 shows the thermodynamically stable phases of the virgin crystals and no low-temperature phases induced by macroscopic strains.

New results were obtained for the $x=0.65$ crystal showing a stable rhombohedral low-temperature phase. This rhombohedral phase can be deduced from the high temperature cubic phase by the compression of one body diagonal and exhibits a large residual entropy as the temperature approaches zero because the CN^- molecules can reorient between three equivalent $\langle 111 \rangle$ directions. In addition to the hindering barriers of the single particle potential of the rhombohedral phase the reorientational motion is hindered by frozen-in strains as demonstrated by the single-crystal diffraction experiments. We are convinced, that the low temperature thermal anomalies in this crystal are due to these properties.

– important results were obtained concerning the static and the dynamic Debye-Waller factors. Specifically we show that the concentration dependence of the static Debye-Waller factors can be explained assuming an interplay of the rotation-translation and the rotation-random strain coupling.

– utilizing single crystal diffraction we performed a careful analysis of the diffuse scattered intensities in mixed crystals just above and below the critical concentration. In both crystals local shear deformations develop due to the interaction of coupled rotational and translational modes with the random strains as introduced by the static impurity centers. We find that the structural phase transition for $x=0.65$ develops out of a crystal with a distribution of apparently frozen-in shear distortions. For $x=0.57$ the local shear deformations are frozen-in due to the dominance of random strains. Analyzing the temperature dependence of the line shapes and of the areas of the diffuse intensities we found a strong increase of the intensities for temperatures below 110 K and a significant anomaly near $T=75$ K. The strong increase of the diffuse intensities can be interpreted as being due to the freezing of shear fluctuations and indicate a nonergodic instability as predicted by Michel [38]. The anomaly near 75 K could be due to residual elastic ordering processes in regions of the crystal exhibiting low random strain fields.

– utilizing high resolution time-of-flight techniques we analyzed the dynamic structure factor for $x=0.57$. The aim was to detect a finite energy width in the quasielastic component (central peak) due to the slowing down of the critical fluctuations in the freezing-in process. We found that the central peak consists of two components: a static component that increases below the glass transition and signals the broken ergodicity of the glass phase and a dynamic contribution that peaks near the glass transition and demonstrates the slowing down of critical strain fluctuations. The results are compared to mode coupling theories which describe the glass transition in supercooled liquids [64–66].

We are grateful to K.H. Michel for numerous discussions and very helpful comments. This work was supported by the German Federal Minister for Research and Technology (Bundesministerium für Forschung und Technologie) under Contract No.: 03-L01MAI-0 (C1-56) and by the Sonderforschungsbereich 262, Mainz (FRG).

References

1. Sullivan, N.S., Devoret, M., Cowan, B.P., Urbina, C.: Phys. Rev. B**17**, 5016 (1978)
2. Rowe, J.M., Rush, J.J., Hinks, D.J., Susman, S.: Phys. Rev. Lett. **43**, 1158 (1979)
3. Loidl, A.: J. Chim. Phys. **82**, 305 (1985)
4. Knorr, K.: Phys. Scr. T**19**, 531 (1987)
5. Press, W., Janik, B., Grimm, H.: Z. Phys. B – Condensed Matter **49**, 9 (1982)
6. Esteve, D., Sullivan, N.S., Devoret, M.: J. Phys. (Paris) **43**, L793 (1982)
7. Klee, J., Carmesin, H.O., Knorr, K.: Phys. Rev. Lett. **61**, 1855 (1988)
8. Grondey, S., Prager, M., Press, W., Heidemann, A.: J. Chem. Phys. **85**, 2204 (1986)
9. Höchli, U.T.: Phys. Rev. Lett. **48**, 1494 (1982)
10. Courtens, E.: Phys. Rev. Lett. **52**, 69 (1984)
11. Lüty, F., Ortiz-Lopez, J.: Phys. Rev. Lett. **50**, 1289 (1983)
12. Loidl, A., Schräder, T., Böhmer, R., Knorr, K., Kjems, J.K., Born, R.: Phys. Rev. B**34**, 1238 (1986)
13. Haussühl, S.: Solid State Commun. **13**, 147 (1973)
14. Michel, K.H., Naudts, J.: Phys. Rev. Lett. **39**, 212 (1977)
15. Rowe, J.M., Rush, J.J., Chesser, N.J., Michel, K.H., Naudts, J.: Phys. Rev. Lett. **40**, 455 (1978)
16. Knorr, K., Loidl, A., Kjems, J.K.: Phys. Rev. Lett. **55**, 2445 (1985)
17. Michel, K.H., Rowe, J.M.: Phys. Rev. B**22**, 1417 (1980)
18. Loidl, A., Feile, R., Knorr, K.: Z. Phys. B – Condensed Matter **42**, 143 (1981)
19. Loidl, A., Feile, R., Knorr, K.: Phys. Rev. Lett. **48**, 1263 (1982)
20. Bhattacharya, S., Nagel, S.R., Fleishman, L., Susman, S.: Phys. Rev. Lett. **48**, 1267 (1982)
21. Rowe, J.M., Rush, J.J., Chesser, N.J.: Ferroelectrics **16**, 107 (1977)
22. Rowe, J.M., Rush, J.J., Susman, S.: Phys. Rev. B**28**, 3506 (1983)
23. Knorr, K., Loidl, A.: Phys. Rev. B**31**, 5387 (1985)
24. Elschner, S., Knorr, K., Loidl, A.: Z. Phys. B – Condensed Matter **61**, 209 (1985)
25. Rowe, J.M., Bouillot, J., Rush, J.J., Lüty, F.: Physica **136**B, 498 (1986)
26. Bouillot, J., Rowe, J.M., Rush, J.J.: Phys. Rev. B**36**, 1766 (1987)
27. Bourson, P., Gorczyca, G., Durand, D.: Cryst. Latt. Def. Amorphous. Mater. **16**, 311 (1987)
28. Mertz, B., Loidl, A.: Europhys. Lett. **4**, 583 (1987)
29. Elschner, S., Albers, J., Loidl, A., Kjems, J.K.: Europhys. Lett. **4**, 1139 (1987)
30. Fossum, J.O., Garland, C.W.: Phys. Rev. Lett. **60**, 592 (1988); Fossum, J.O., Wells, A., Garland, C.W.: Phys. Rev. B**38**, 412 (1988)
31. Garland, C.W., Kwiecien, J.Z., Damien, J.C.: Phys. Rev. B**25**, 5818 (1982)
32. Feile, R., Loidl, A., Knorr, K.: Phys. Rev. B**26**, 6875 (1982)
33. Loidl, A., Feile, R., Knorr, K., Kjems, J.K.: Phys. Rev. B**29**, 6052 (1984); Loidl, A., Knorr, K., Feile, R., Kjems, J.K.: Phys. Rev. Lett. **51**, 1054 (1983)
34. Loidl, A., Müllner, M., McIntyre, G.J., Knorr, K., Jex, H.: Solid State Commun. **54**, 367 (1985)
35. Loidl, A., Knorr, K., Rowe, J.M., McIntyre, G.J.: Phys. Rev. B**37**, 389 (1988)
36. Knorr, K., Loidl, A.: Phys. Rev. Lett. **57**, 460 (1986)
37. Michel, K.H.: Phys. Rev. Lett. **57**, 2188 (1986); Phys. Rev. B**35**, 1405 (1987); Phys. Rev. B**35**, 1414 (1987)
38. Michel, K.H.: Z. Phys. B – Condensed Matter **68**, 259 (1987); Bostoen, C., Michel, K.H.: Z. Phys. B – Condensed Matter **71**, 369 (1988)
39. For a review see DeYoreo, J.J., Knaak, W., Meissner, M., Pohl, R.O.: Phys. Rev. B**34**, 8828 (1986)
40. Berret, J.F., Doussineau, P., Levelut, A., Meissner, M., Schön, W.: Phys. Rev. Lett. **55**, 2013 (1985)
41. Moy, D., Dobbs, J.N., Anderson, A.C.: Phys. Rev. B**29**, 2160 (1984)
42. Anderson, P.W., Halperin, B.I., Varma, C.M.: Philos. Mag. **25**, 1 (1972)
43. Phillips, W.A.: J. Low. Phys. **7**, 351 (1972)
44. Meissner, W., Knaak, W., Sethna, J.P., Chow, K.S., DeYoreo, J.J., Pohl, R.O.: Phys. Rev. B**32**, 6091 (1985); Sethna, J.P., Chow, K.S.: Phase Transitions **5**, 317 (1985); Sethna, J.P.: N.Y. Acad. Sci. **484**, 130 (1987);

Grannan, E.R., Randeria, M., Sethna, J.P.: Phys. Rev. Lett. **60**, 1402 (1988)
45. Nicholls, C.I., Yadon, L.N., Haase, D.G., Conradi, M.S.: Phys. Rev. Lett. **59**, 1317 (1987)
46. Lewis, L.J., Klein, M.L.: Phys. Rev. Lett. **57**, 2698 (1986); J. Phys. Chem. **91**, 4990 (1987)
47. Lewis, L.J., Klein, M.L.: Phys. Rev. Lett. **59**, 1837 (1987)
48. Goldbart, P., Sherrington, D.: J. Phys. C **18**, 1923 (1985)
49. Kanter, I., Sompolinsky, H.: Phys. Rev. B **33**, 2073 (1986)
50. Carmesin, H.O., Binder, K.: Z. Phys. B – Condensed Matter **68**, 375 (1987)
51. Truthe, W.: Z. Anorg. Chem. **76**, 129 (1912) In this work the x, T-phase diagram of KCl:KCN mixed systems is given; due to the similar high melting point of KCl and KBr, as compared to KCN, we believe that the KBr:KCN phase diagram looks very similar
52. Kaack, J.: Diplomarbeit, Universität zu Köln, Köln (1980)
53. Suga, H., Matsuo, T., Seki, S.: Bull. Chem. Soc. Jpn. **38**, 1115 (1965)
54. Lüty, F.: In: Defects in insulating crystals. Turkevitch, V.M., Svarts, K.K. (eds.), pp. 69–89. Berlin, Heidelberg, New York: Springer 1981
55. Matsuo, T., Kishimoto, I., Suga, H., Lüty, F.: Solid State Commun. **58**, 177 (1986)
56. Knorr, K., Civera-Garcia, E., Loidl, A.: Phys. Rev. B **35**, 4998 (1987)
57. Parry, G.: Acta Crystallogr. **15**, 601 (1961)
58. Jäckle, J.: Rep. Prog. Phys. (1986)
59. Rietveld, H.M.: J. Appl. Crystallogr. **2**, 65 (1969)
60. Hewat, A.W.: Harwell Report AERE-R7350 (1973)
61. Knopp, G., Knorr, K., Loidl, A., Haussühl, S.: Z. Phys. B – Condensed Matter **51**, 259 (1983)
62. Folk, R., Iro, H., Schwabl, F.: Z. Physik B – Condensed Matter and Quanta **25**, 69 (1976); Phys. Rev. B **20**, 1229 (1979)
63. Zeyen, C.M., Chagnon, R., Disdier, F., Morin, H.: Rev. Phys. Appl. **19**, 789 (1984)
64. Leutheusser, E.: Phys. Rev. A **29**, 2765 (1984)
65. Bengtzelius, U., Götze, W., Sjölander, A.: J. Phys. C **17**, 5915 (1984); Götze, W., Sjögren, L.: Z. Phys. B – Condensed Matter **65**, 415 (1987)
66. Bernu, B., Hansen, J.P., Hiwatari, Y., Pastore, G.: Phys. Rev. A **36**, 4891 (1987)
67. Volkmann, U.G., Böhmer, R., Loidl, A., Knorr, K., Höchli, U.T., Haussühl, S.: Phys. Rev. Lett. **56**, 1716 (1986); Loidl, A., Knorr, K.: Ann. NY Acad. Sci. **484**, 121 (1986)
68. Doverspike, M.A., Wu, M.-C., Conradi, M.S.: Phys. Rev. Lett. **56**, 2284 (1986)

A. Loidl, T. Schräder, K. Knorr, R. Böhmer, B. Mertz
Institut für Physik
Universität Mainz
Staudinger Weg 7
D-6500 Mainz
Federal Republic of Germany

G.J. McIntyre
The Studsvik Neutron Research. Lab.
University of Uppsala
S-61182 Nyköping
Sweden

T. Vogt, H. Mutka
Institut Max von Laue-Paul Langevin
Avenue des Martyrs-156 X
F-38042 Grenoble Cedex
France

M. Müllner
Institut für Kernphysik
Univeristät Frankfurt
August-Euler-Strasse 6
D-6900 Frankfurt am Main 90
Federal Republic of Germany